ELSEVIER

Contents lists available at ScienceDirect

Applied Materials Today

journal homepage: www.elsevier.com/locate/apmt



Ultrafast assembly and healing of nanomaterial networks on polymer substrates for flexible hybrid electronics

Dong Zhou a,b, Meikang Han c, Bchara Sidnawi a,d, Qianhong Wu a,d, Yury Gogotsi c, Bo Li a,b,*

- ^a Department of Mechanical Engineering, Villanova University, Villanova, PA 19085, USA
- b Hybrid Nano-Architectures and Advanced Manufacturing Laboratory, Villanova University, Villanova, PA, 19085, USA
- ^cA. J. Drexel Nanomaterials Institute and Department of Materials Science and Engineering, Drexel University, Philadelphia, PA 19104, USA
- ^d Cellular Biomechanics and Sports Science Laboratory, Villanova University, Villanova, PA, 19085, USA

ARTICLE INFO

Article history: Received 10 October 2020 Revised 10 January 2021 Accepted 21 January 2021

Keywords: Assembly Healing Dip coating Sonication Self limiting

ABSTRACT

High throughput manufacturing of regenerable nanomaterial-based flexible electronics represents an extreme challenge. Here we demonstrate a rapid and eco-friendly assembly and regeneration of nanomaterial networks (films) on a hydrophobic polymer substrate (i.e., polydimethylsiloxane) from a sonicated dispersion of hydrophobic nanoparticles in water. The self-limiting sono dip coating (SDC) assembly is characterized by an ultrafast withdrawal speed (16 m/min, one to five orders of magnitude greater than that of existing nanomaterial dip-coating processes) and insensitivity to substrate geometry. It is applicable to a wide range of hydrophobic nanomaterials, from graphene to carbon nanotubes and poly (methyl methacrylate) nanoparticles. The sono healing method requires only 1 min sonication in water to regenerate graphene/polydimethylsiloxane strain sensors. Furthermore, the SDC can be combined with other nanomaterial deposition methods (e.g., electroplating) to build heterostructures and integrated devices.

© 2021 Elsevier Ltd. All rights reserved.

1. Introduction

Nanomaterial-based flexible electronics (NFEs) that integrate the functionality of nanomaterials and the flexibility of polymer substrates promise to revolutionize a wide range of industries, from electronics [1-3] and energy [4-6] to healthcare [7,8]. The potential health and environmental concern of releasing nanomaterials and polymers into the environment and the use of toxic solvents and agents in the manufacturing process presents a significant challenge for next-generation manufacturing technologies. Eco-manufacturing represents an important trend for the advanced manufacturing of NFEs, in which researchers not only consider the technical challenges of integrating two drastically different components in a high throughput manner, they also address the issues related to the energy consumption, health and environmental impacts over the entire device lifecycle. On the one hand, it is necessary to achieve high-rate, eco-friendly, and low-cost nanomanufacturing. Development of high-throughput assembly methods (e.g., dip coating [9], drop coating [10], spin coating [11], and meniscusassisted assembly [12]) represents a major thrust forward in efforts using bottom-up strategies. The question how to recycle these

NFEs towards the end of their lifecycle, preventing the release of nanomaterials and polymer waste into the environment, remains critical. While self-healing methods have drawn significant attention in recent years [13–17], their practical applications are limited and a strategy for repair and regeneration, similar to the ones widely used in repairing damaged metals and ceramics at the macroscopic scale [18], is lacking.

In this paper, we have combined an interfacial energy design of a nanomaterial-polymer-solvent system with a sono-matter interaction mechanism, to achieve ultrafast assembly and healing of a nanomaterial network on a polymer substrate using deionized (DI) water as the solvent. This research resulted in the invention of an ultrafast but self-limiting sono dip coating (SDC) method and the creation of a new sono-healing protocol. Unlike the traditional dip-coating assembly process, where the withdrawal speed and assembly efficiency are restricted by the slow solvent evaporation. In this SDC method, the film is directly formed in the solution. And because the assembled nanomaterial film is hydrophobic, water will not stick to the film during the withdrawal, and therefore, the evaporation process is eliminated. As a result, the withdrawal speed of SDC can reach 16 m/min which is 1 to 5 orders of magnitude higher than any other nanomaterials dip-coating system [19-25] and at least an order of magnitude higher than the maximum speed of commercial desktop dip-coaters [26]. Because of the elimination of the evaporation process, cyclic dip coating can be per-

^{*} Corresponding author.

E-mail address: bo.li@villanova.edu (B. Li).

formed continuously to control the thickness and coverage of the assembled film. We have found that the assembly is a self-limiting process; the assembled film thickness and resistance quickly reach a plateau. Importantly, the nanomaterial network that was damaged after mechanical deformations can recover its conductivity and regenerate its functionality through a simple, one-minute-long, sono-healing treatment. Further, the assembly method can be integrated with other manufacturing processes, making it suitable for fabricating integrated circuits and realizing a wide range of functionalities. As a proof-of-concept, we have demonstrated the electroplating of MXene and Ni on the graphene-coated PDMS substrate, for electromagnetic interference (EMI) shielding and a solid-state flexible capacitor. This work paves the way towards rational design and eco-manufacturing of large scale, integrated, reusable, and affordable flexible electronics.

2. Material and methods

2.1. Materials

The SYLGARDTM 184 (PDMS) was provided by Dow Corning Corp. Graphene grade M5 (~5 µm in lateral dimension and 6-8 nm in thickness, \sim 120 to 150 m²/g) was purchased from XG-Sciences. The multi-walled carbon nanotube (outer diameter: 50-80 nm, CAS# 99685-96-8) was purchased from US Research Nanomaterials, Inc. MoS₂ and h-BN were purchased from Sigma-Aldrich. The carbon black (Asbury nano 24) was purchased from the Asbury Cabons Inc. The graphene oxide (GO) was prepared according to the modified Hummers method [27]. The as-prepared graphene oxide was dried by heating at 80 °C for 48 h. All chemicals used were purchased from Sigma-Aldrich and used as received without further purification. Then, the graphene oxide was annealed at 800 °C for 4 h under the argon/H₂ (85/15) atmosphere. The XRD patterns for as-prepared GO and rGO are shown in Fig. S1 in the Supplementary Information. Ti₃C₂T_x MXene was synthesized by the selective etching of Al form Ti₃AlC₂ powder using the approach reported in our previous work [28]. The experimental details can be found in the Supplementary Information.

2.2. Sono dip-coating assembly

In all cases, the sonication was performed using an ultrasonic cleaner (JP-010S) sonicator with a frequency of 40 kHz and a chamber size of 150 mm \times 135 mm \times 10 mm. The output power is 60 W and the sono energy is determined by the ratio of the output power to the cross-sectional area of the chamber. All the assembly processes were taken under 50 °C. There are two reasons why we choose 50 °C as the assembly temperature. (1) The sonication will generate energy and increase the temperature during the assembly process. We found 50 °C is a proper temperature that the sonicator can maintain. (2) the higher exfoliation temperature for graphene shows a more stable solution [29]. Briefly, the nanomaterials with various weights added into 100 ml DI water in a beaker, and the solution was sonicated for 1 h before the assembly. The rotation speed is fixed at 60 rpm to get a fixed period of 1 s. In each assembly cycle, the real assembly time (0.5 s) is defined as the time frame between the sample's bottom arriving and leaving the nanomaterials solution, as marked in Fig. 2b.

2.3. Nickel plating

For the Nickel plating, 3 g of ammonium nickel (II) sulfate hexahydrate (\geq 98%) was dissolved in 100 ml DI water and sonicated for 10 min to obtain a clear solution. The graphene/PDMS was connected to the negative electrode of the power station (EVENTEKTM KPS3010DF), and the positive electrode was connected to a Ni plate

and then inserted the Ni plate into the solution. A 5 V bias was applied until the full coverage of Ni on the graphene surface, which can be easily identified through the color contrast. The hybrid Ni/graphene/PDMS was pulled up once the plating process completed.

2.4. MXene plating

The MXene solution was used as-synthesized with a concentration of 2 mg/ml. 100 ml solution was added into a 100 ml beaker, and the graphene/PDMS was connected to the positive electrode of the power station. The negative electrode was connected to the solution and far away from the sample. A 15 V bias was applied for 5 min then the plated sample was pulled out slowly and dried in air for 24 h.

2.5. Fabrication of MXene/graphene/PDMS supercapacitor

For the flexible supercapacitor, PVA-KOH gel electrolyte was prepared by dissolving 3 g of PVA (weight-averaged molecular weight $M_{\rm W}$ 146,000–186,000, 99% hydrolyzed) powder in 40 ml of DI water at 90 °C under vigorous stirring. 3 g of KOH (≥85%) was dissolved in 10 ml of DI water at room temperature and then added into the PVA solution. The mixed solution was cooled down to room temperature and poured into a rolled PET mold with a fixed cylinder MXene/graphene/PDMS as the inner electrode. The solution was frozen overnight and thawed at room temperature for 1 h, and then a homogenous gel was achieved. A piece of rectangular MXene/graphene/PDMS was cut and rolled onto the surface of the prepared gel, and a Kapton tape encapsulated the whole device. The dimensions of the prepared PVA/KOH electrolyte were 5, 10, and 12.7 mm for the inner diameter, outer diameter, and height, respectively. The fabrication of the graphene/PDMS reference device follows the same procedure except replacing the MXene/graphene/PDMS electrodes with graphene/PDMS electrodes.

2.6. Characterizations

The contact angle measurement was conducted using a goniometer (SEO Contact Angle Analyzer, Alpha 1). SEM images were taken using a Hitachi S-4800 SEM. The electrical properties were measured by using a Keithley 2400 source meter. The sheet resistance was tested by a four-probe method. The resistance measurements were conducted through the two-probe method. Briefly, samples were cut into a size of $\sim 25 \text{ mm} \times 5 \text{ mm} \times 1 \text{ mm}$, and silver paint was applied to both ends of the samples and dried for 24 h before the tests. The sensing behavior and long-term stability testes of the strain sensors tests were performed using a Psylothch μ TS test system together with a Keithley 2400. A rectangular sample was fixed on the two clamps of the tensile tester system with a 10 mm gap. For the sensing behavior under different strains, in order to keep the same testing period, the strain speeds of 0.5, 1.0, 2.0, 4.0, 10.0 and 20.0 µm/s were used for the strains of 0.25, 0.5, 1, 2, 5 and 10%, respectively. For each strain, the sample was cycled 10 times. The resistance change during the stains was recorded synchronously. The long-term stability testing was performed under the strain of 1% with a speed of 1 μ m/s. The optical images were taken using an Olympus BX51M optical microscope. The thickness of the assembled film was characterized by a commercial confocal laser scanning microscope (VKx 1100, Keyence, Osaka, Japan). EMI shielding performance was calculated using Sparameters (The calculation details are in the Supplementary Information). S-parameters were measured using a vector network analyzer (VNA; 8720ES, Agilent) with a WR-90 rectangular waveguide in the X band (8.2–12.4 GHz). The capacitance was measured by an LCR meter (GW Instek LCR-6100). The specific capacitances

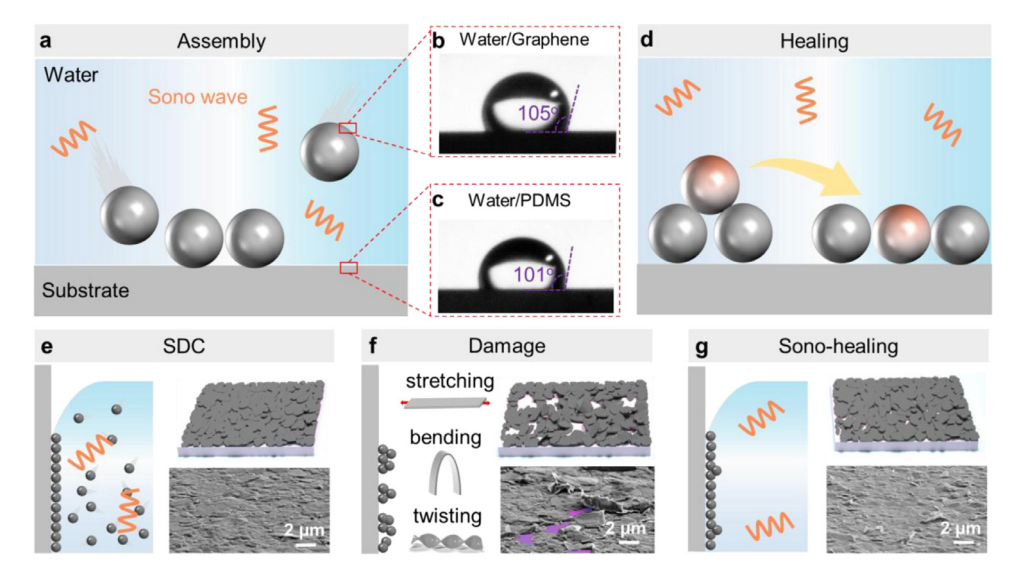


Fig. 1. Schematic of assembly and healing processes. (a) Schematic of the particle assembly at the water-substrate interface driven by low interfacial energy and weak sono wave. (b) Water contact angle on the assembled graphene film surface. (c) Water contact angle on the PDMS surface. (d) Schematic of the healing process where stacked particles are reorganized into a film; Particles prefer to stay on the surface of polymer substrate and be reorganized by the forces generated by weak sono wave. (e) Schematic of the SDC process and a graphene film assembly on PDMS. (f) Schematic of the mixed deformation processes and the resultant damaged graphene network on PDMS. The SEM image shows the delamination and cracks (pink regions) on graphene film. (g) Schematic and SEM image of the healed sample by applying the sono-healing.

of the cylinder capacitor were calculated by normalizing the capacitance to the inner surface area of PVA electrolyte.

3. Results and discussion

3.1. Assembly and healing mechanism

As shown in Fig. 1a-d, the combined interfacial energy and sono-matter interaction mechanism can be applied for both, the assembly and healing processes. Here, we simply use spherical particles to represent the nature of network arrangement during assembly and healing while two dimensional (2D) flakes and one dimensional (1D) tubes/wires will enable additional mechanisms, e.g., stacking and entanglement, for network evolvement. First, we design a nanomaterial-solvent-polymer system with higher interfacial energies for solvent-polymer and solvent-nanomaterials and lower interfacial energy for nanomaterial-polymer to meet the thermodynamic principle that the formation of the nanomaterialspolymer interface is energetically favorable (Fig. 1a). We use graphene-water-polydimethylsiloxane (PDMS) as a demonstration system. The contact angles of water on graphene film (assembled on PDMS) and water on pure PDMS are shown in Figs. 1b and 1c, respectively. The contact angle measurements demonstrate the hydrophobic nature of the graphene and PDMS, along with the corresponding higher interfacial energy, between water and graphene ($\gamma_{\text{water-graphene}} = 13.89 \text{ mJ/m}^2$), as well as between water and PDMS ($\gamma_{\text{water-PDMS}} = 38.84 \text{ mJ/m}^2$). The interfacial energy between graphene and PDMS ($\gamma_{graphene\text{-PDMS}} = 11.62 \text{ mJ/m}^2$) is calculated to be the lowest suggesting that the assembly process is energetically preferred (see Supplementary Information for detailed calculation and, Tables S1 and S2 for different nanomaterial systems). Secondly, a weak sono field is introduced to enhance the nanomaterial-polymer collision and nanomaterial dispersion through the acoustic force [30], the streaming flow [31,32], and the microjets generated by the collapse of cavitation [33]. It is also important to note that the weak sono field-induced forces can also reorganize the assembled nanomaterial network [34], which is the key mechanism for healing the nanomaterial network after damage (Fig. 1d).

Based on these principles, we have developed an ultrafast and self-limiting SDC technique, as shown in Fig. 1e. Because of the choice of hydrophobic substrate and nanomaterials, the contact angle of the water-based solution is higher than 90°. Unlike the traditional dip-coating process where the deposition happens at the frontier of the solid (substrate)-liquid-vapor contact line and is driven by the solution evaporation, the assembly of SDC occurs at the solid-liquid interface in the solution instead. The combination of the lower interfacial energy of the nanomaterial-polymer interface and the enhanced collision between the nanomaterial and the polymer through a weak sono field (0.3 W/cm²) guarantees a rapid assembly of nanoparticles. The withdrawal speed can be as high as 16 m/min for the current design, which is orders of magnitude higher compared to the existing dip-coating processes for nanomaterials (see Supplementary Information for detailed comparison and Table S3) and at least 16 times higher than the upper speed limit of most commercial dip-coaters (50-1000 mm/min, Table S4, Supplementary Information). Furthermore, the substrate with assembled nanomaterial film is withdrawn from the solution without evaporation of extra solvent during the process, as both PDMS and nanomaterials are hydrophobic. Therefore, a cyclic dip coating can be performed continuously to control the coverage and thickness of the nanomaterial film. As an example, the scanning electron microscope (SEM) image of the continuous graphene film assembled on the PDMS substrate (0.5 mg/ml, 200 cycles, 9.6 m/min of withdrawal speed) is shown in Fig. 1e. The PDMS surface is fully covered by graphene flakes. The detailed assembly process and the mechanism of SDC, along with and its scalability to different materials, scales, and substrate geometries, will be discussed in Fig. 2.

The healing process also utilizes these two principles. The difference is that no nanomaterial is required in the solution (pure DI water), as shown in Fig. 1d. While energetically, nanomaterials tend to stay on the polymer substrate rather than going back to the solution, the forces induced by the weak sonication help reorganize the damaged nanomaterials network. In comparison, the same sample in Fig. 1e is damaged through randomly mixed deformations (stretching, bending, and twisting), leading to stacks of flakes and exposed PDMS areas (pink regions in Fig. 1f) due to the delamination and reorganization of graphene flakes. After 1 min of sono-healing treatment (0.3 W/cm²) in DI water, the network can

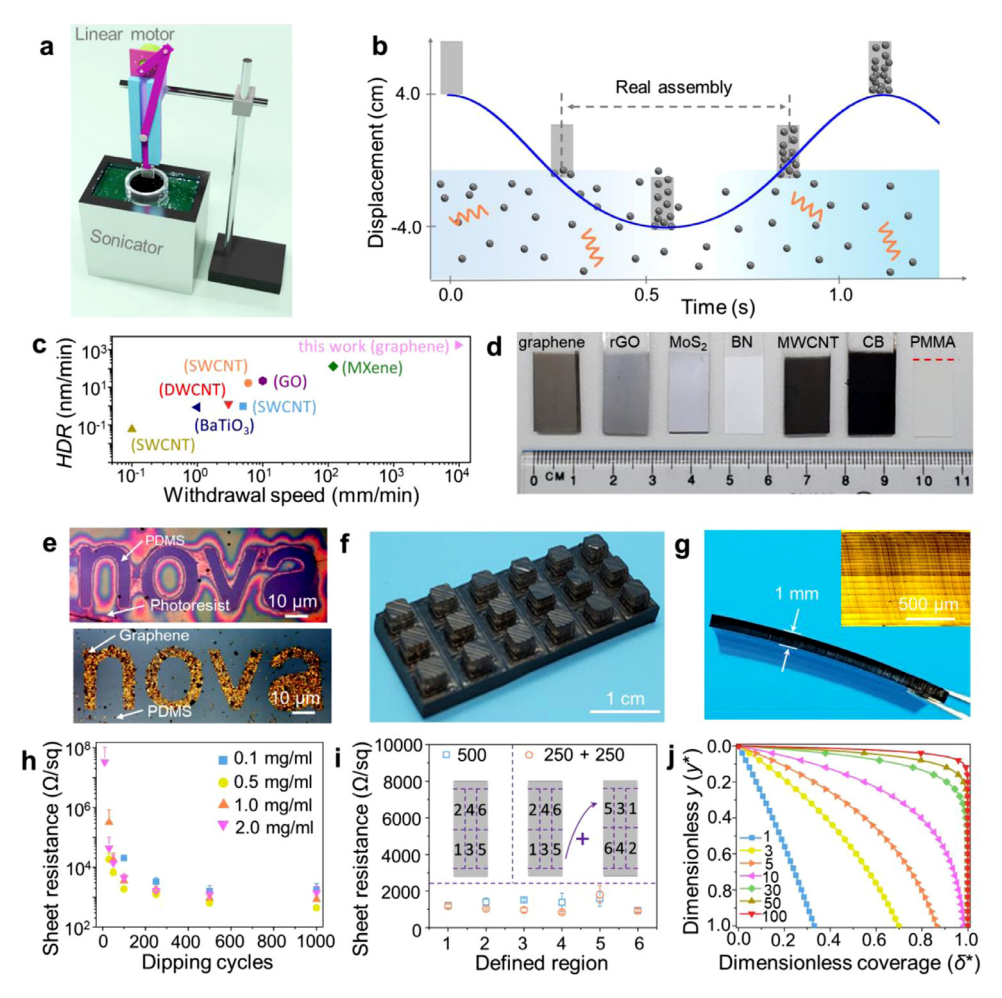


Fig. 2. The schematic and assembly capability of SDC. (a) Schematic of the customized dip coater for SDC. (b) Displacement of the polymer substrate with respect to time in one assembly cycle. (c) The comparison of the highest deposition rate (HDR) versus withdrawal speed between this work and traditional dip coating. (d) Assembly of different nanomaterials, i.e., graphene, reduced graphene oxide, MoS₂, h-BN, carbon nanotubes, carbon black, and PMMA nanoparticles. (e) Microscale assembly of graphene into the word "nova". (f) Graphene assembly on a 3D macro-patterned PDMS surface. (g) A multilayer graphene/PDMS composite through alternating spin-coating and SDC. The inset shows the optical image of the cross-sectional view. (h) Sheet resistance versus dipping cycle under different solution concentrations. (i) The sheet resistance of six different locations under two different dipping modes; the "500" means that the substrate goes through 500 dipping cycles continuously, and the "250 + 250" means that the substrate is turned upside down after 250 cycles and runs another 250 cycles; the inset shows the defined six regions on the assembled samples. (j) The simulated assembly distribution over the substrate under different dipping cycles.

be recovered (Fig. 1g). The functionality of a hybrid device can be regenerated, and a proof-of-concept demonstration of a healable strain sensor will be further explored in Fig. 3.

3.2. Sono dip-coating assembly

The ultrafast SDC assembly is realized through a customized slider-crank mechanism (Fig. S2, Supplementary Information), printed using a Lulzbot TAZ 6 Desktop 3D Printer and driven by a linear DC motor, as shown in Fig. 2a. A representative displacement versus time curve is shown in Fig. 2b. The corresponding average withdrawal speed (the same as the dipping speed in the current design) is 9.6 m/min at the angular velocity of 60 rpm (the calculation details can be found in Supplementary Information). The displacement of the specimen is shown in the blue curve in Fig. 2b. The maximum average withdrawal speed can reach 16 m/min through this design with a maximum angular speed of 100 rpm. It is important to notice that, this speed limit is determined by the current combination of the motor and the slidercrank mechanism and is not the upper-speed limit of the SDC method. Further improvement can be achieved by adjusting the motor and the design of the mechanism. There is a possibility that

the true speed limit may be determined by the fluid shearing effect caused by the rapid movement of the substrate in the solution, which is worthy of further exploration. Fig. S3 shows film thickness versus dipping cycles with a solution concentration of 0.5 mg/ml and a withdrawal speed of 9.6 m/min suggests a rapid deposition during the first 100 cycles and film thickness reaches a plateau (~140 nm) after 400 cycles. We have also compared the withdrawal speed and the highest deposition rate (HDR) between SDC and traditional dip coating, as shown in Fig. 2c and Table S3, Supplementary Information. $HDR = c^*h/t^*$, where h is the deposited film thickness, c* is a concentration correction factor (defined as the actual solution concentration divided by 1 mg/ml), and t^* is defined as the time to complete a 3 cm long sample (which is the same sample size in our SDC assembly). The HDR of our work is calculated based on 10-cycle assembly (at withdrawal speed of 9.6 m/min, and concentration of 0.5 mg/ml) which leads to a 75 nm thick graphene film (Fig. S3, Supplementary Information). Our work not only has the highest withdrawal speed (1 to 5 orders of magnitude higher), but also has the highest HDR (1 to 4 orders of magnitude higher) compared to that of the traditional nanomaterial dip coatings. To obtain a reasonable comparison, we have chosen the nanomaterials with similar dimension compared to graphene

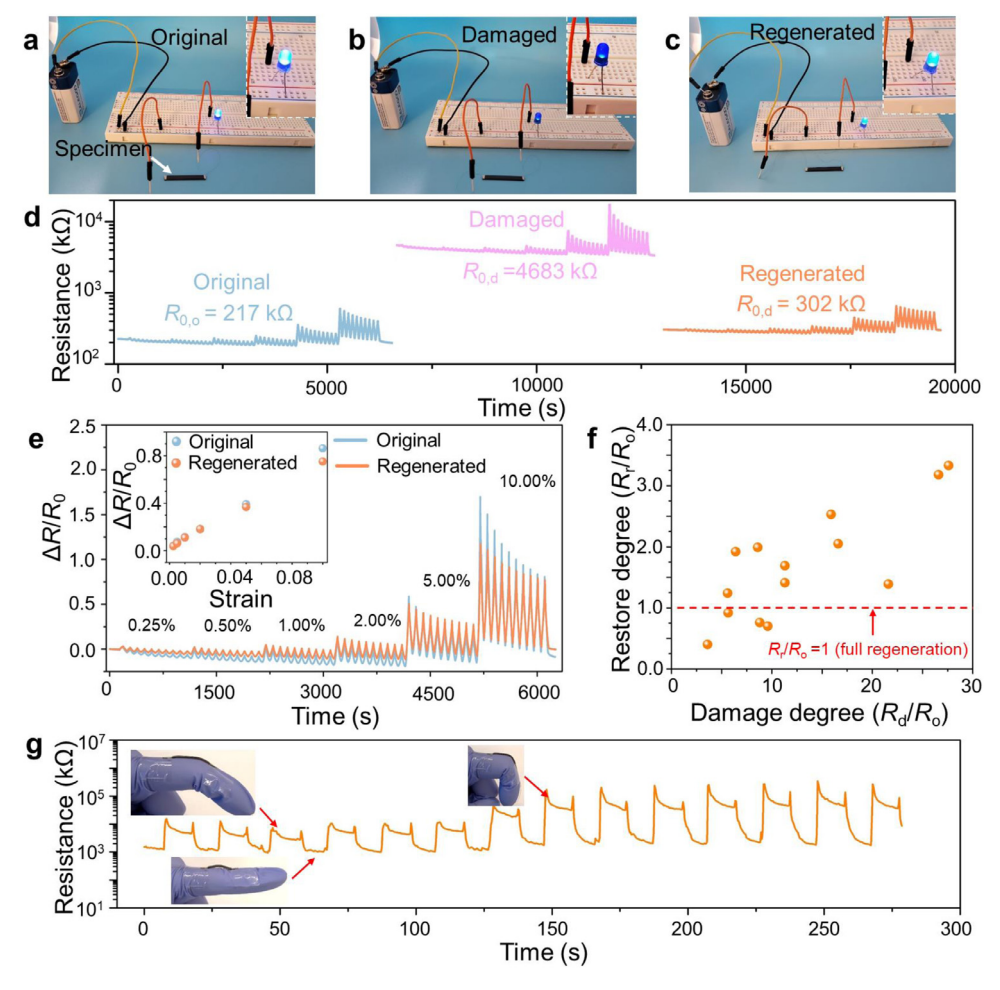


Fig. 3. Sono-healing and regeneration of damaged flexible devices. (a-c) The lightening of a diode with the original, damaged, and regenerated graphene/PDMS resistor, respectively. (d) A representative resistance changing under various strains from 0.25 to 10% for the same graphene/PDMS specimen with different statuses: original, damaged, and regenerated. (e) The relative resistance (Δ R/R0) for original and regenerated graphene/PDMS under various strains; the inset shows that the relative resistance increases monotonically up to 10% strain. (f) The healing coefficient (Rr/R0) versus the damage degree (Rd/R0) of randomly damaged samples. (g) The response of the bending of the index finger under different angles using an as-assembled graphene/PDMS strain sensor. Insets show the bending and extending movements of the index finger.

nanosheets in the thickness direction, and therefore, graphene oxide (GO) [19], single-walled carbon nanotubes (SWCNT) [9,21,22], double-walled nanotubes (DWCNT) [23], BaTiO₃ nanosheets [24], and MXene (Ti₃C₂T_{χ}) [25] were chosen. The detailed information can be found in Table S3 in the Supplementary Information.

In addition to the ultrafast withdrawal speed, SDC has several other unique characteristics. First, it can be generalized to a wide range of inorganic and organic particles with different geometries. In Fig. 2d, we show a collection of nanomaterials assembled on a PDMS substrate, including inorganic nanomaterials, e.g., 2D graphene, reduced graphene oxide (rGO), molybdenum disulfide (MoS₂), boron nitride (h-BN), 1D multi-walled carbon nanotubes (MWCNTs), 0D carbon black (CB), and organic poly(methyl methacrylate) (PMMA) nanoparticles. For comparison of all nanomaterials, the withdrawal speed, the solution concentration, and the dipping cycle were set as 9.6 m/min, 0.5 mg/ml, and 200 times, respectively. The SEM images of the assembled films (graphene, rGO, MWCNT, and CB) can be found in Fig. S4 in the Supplementary Information. Secondly, we have also demonstrated the highly accurate and selective assembly of graphene on a micropatterned PDMS surface, forming a word "nova" with a line width of 5 μ m. The pattern is defined through a photolithography process (Fig. 2e and Fig. S5, Supplementary Information), demonstrating the compatibility of SDC with microfabrication technologies. Thirdly, SDC is not sensitive to surface geometries, and a continuous assembly of graphene can be achieved on complex macro-patterned 3D PDMS substrates (with pillars and curved features), as shown in Fig. 2f and Fig. S6 in the Supplementary Information. In contrast, in traditional dip coating, the surface geometry may affect the uniformity/continuity of the assembly, because it changes the solution wetting and the evaporation rate [35–37]. Fourth, the ultrafast nature of the assembly method enables the capability of building a hierarchical structure for further functionalization. As a proof-of-concept, we stacked 20 layers of assembled graphene/PDMS composite within 1 mm thickness by alternating PDMS coating and graphene assembly, as shown in Fig. 2g and Fig. S7 in the Supplementary Information. Each PDMS layer with controlled thickness is fabricated by spin-coating the mixed monomer and curing agent and then cured at 120 °C for 5 min.

Lastly, SDC is a self-limiting assembly process that guarantees the uniform assembly of nanomaterials on the polymer substrate. The self-limiting effect is identified with the increased dipping cycles and across the entire substrate. In Fig. 2h, a sharp decrease of sheet resistance (at different solution concentrations) happens after the first 100 cycles and the curves start to flatten out after 200 cycles, reaching a plateau after 500 cycles. This trend is similar to the variation of the thickness of assembled graphene film, as shown in Fig. S3 in the Supplementary Information. The comparison among different curves shows that the concentration of solution has little influence on the sheet resistance after 200 cycles,

suggesting a self-limiting process. While a continuous conductive network can form already after 10 dipping cycles in the solution of 2.0 mg/ml, which corresponds to 5 s exposure to the solution, it is difficult to achieve a good uniformity of the film. This is because the bottom part of the substrate may be immersed in the solution longer than the top, leading to a thickness gradient, as shown in Fig. 2b. However, the self-limiting nature of the process eventually increases the uniformity of the film over the substrate with the increased number of dipping cycles. It is confirmed by the sheet resistances measured in six different locations, which shows similar values under two different dipping modes (Fig. 2i). In mode one, the substrate went through 500 dipping cycles continuously, and in mode two, the substrate was turned upside down after 250 cycles and finished at 500 cycles. For each mode, six different regions show similar sheet resistances, and for each region, the values from two modes are also similar. The reported sheet resistances in Fig. 2h are the average values of six different locations of the samples. The film thickness dependence on the number of dip-coating cycles in 0.5 mg/ml solution is shown in Fig. S3 in the Supplementary Information. After 500 cycles, the thickness of the film also reaches a plateau of 140 nm. A probabilistic approach is adopted to explain this self-limiting mechanism [38], and the simulation result is presented in Fig. 2j. $y^* = 1$ and $y^* = 0$ are the dimensionless coordinate values at the lower and upper ends of the substrate, respectively. δ^* is the dimensionless surface coverage (density) and $\delta^* = 1$ means complete coverage. We assume that the probability of a particle attaching to the substrate after colliding with it, is a function of the particle's head-on (perpendicular to the substrate), and sideways velocity (parallel to the substrate) components upon impact, and the soft polymer surface that can absorb the kinetic energy is the preferred surface for nanomaterial assembly. This probability function would be expected to be defined by the chosen nanomaterial solution and the substrate material. For the current solution concentration during the current cycle, and the set sonication conditions, this probability would imply a certain frequency, $f(1/(m^2 \cdot s))$ at which the substrate's exposed area is capturing the particles. Intuitively, this frequency is proportional to the solution concentration, c (kg/m³) resulting from the previous dip, $f = \alpha c$, where α (m/(kg.s)) is the proportionality constant. Depending on the particle size and mass, for one layer of nanoparticles, there is a maximum surface density that can be achieved. As the surface density towards the lower end approaches its maximum with further dips, the substrate's exposed area will shrink enough to allow the upper regions to catch up. Eventually, a uniform layer of nanoparticles will stick to the substrate before further layers start forming (100 cycles, red curve). The parameter α can be modeled as a decreasing function of the number of layers, which asymptotically approaches zero at infinity, thereby eventually preventing further growth.

3.3. Sono-healing of damaged films

Advanced manufacturing technology to repair and regenerate NFEs will be crucial for sustainable and affordable applications of NFEs. Here, using graphene-PDMS devices, we demonstrate that sono-healing not only recovers the nanomaterials network but also regenerates the device functionality. The healing process was performed by putting the damaged graphene/PDMS devices back to pure DI water with sonication for 1 min. Considering the complex deformation in the practical applications of an NFE device, we used a combined stretch-twist method to initiate the network damage. We first demonstrated the regeneration of the function as a resistor, as shown in Fig. 3a-c. The lightening of a diode with original, damaged, and regenerated graphene/PDMS resistor, is compared. The recovered light intensity is the direct evidence of function recovery. The SEM images in Fig. 1e-g also indicated the damage and

reconstruction of the conductive network. We have also demonstrated the regeneration of more complicated strain sensing capability, as shown in Fig. 3d-f. Fig. 3d tracks the resistance change under various strains from 0.25 to 10% for the same specimen with different statuses: original (blue), damaged (purple), and regenerated (orange) statuses. The baseline or initial resistance (R_0) increases from 217 k Ω ($R_{0,0}$, original) to 4683 k Ω ($R_{0,d}$, damaged), and then recovers to 302 k Ω ($R_{0,r}$, regenerated). Although $R_{0,r}$ is slightly higher than $R_{0,0}$, their sensing behavior and gauge factor are very similar, as shown in Fig. 3e. The relative resistance ($\Delta R/R_0$, where $\Delta R = R - R_0$; R and R_0 represent the resistance after deformation and the initial resistance of the strain sensor, respectively) was plotted as a function of time. The inset shows that the relative resistance (R and R_0 were defined as the peak resistance and the initial resistance of the strain sensor in the last cycle under each strain, respectively) under different strains increases monotonically up to 10 %. However, for the damaged sample, the relative resistance increases nonmonotonically when the strain exceeds 5 %, indicating the instability of the damaged sample (Fig. S8, Supplementary Information). Gauge factors (GF) have been determined by fitting the linear region corresponding to 8.2 and 7.2 for the original and regenerated samples, which indicates the excellent recovery. The sono-healing can accommodate a wide range of damage as shown in Fig. 3f. R_d/R_0 is defined as the damage degree, where R_d is the sample resistance after random stretching and twisting. Correspondingly, we have defined a healing coefficient R_r/R_0 (R_r is the regenerated resistance). Healing coefficient $R_r/R_0 = 1$ means full regeneration (red dash line, Fig. 3f). It is interesting to note that for damage degree less than 10, full regeneration or even enhanced conductive network $(R_r/R_0 < 1)$ can be realized. For more severe damage (e.g., $R_d/R_0 = 26.6$), the healing process can recover the resistance close to its original resistance ($R_r/R_0 = 3.2$). At last, as a proof of concept, a graphene-PDMS flexible sensor is attached to the index finger to detect the gesture of the finger (Fig. 3g), and the long-term stability of the strain sensor under 1 % strain is explored (Fig. S9, Supplementary Information). It demonstrates the stability of the flexible sensor.

3.4. Building integrated devices

To further build integrated circuits or functional devices, the capability of the SDC to integrate with other manufacturing processes is critical. As a proof of concept, we have demonstrated the combination of SDC with electroplating to fabricate hierarchical devices for enhanced functionalities in which Ni and MXene layers were deposited on top of graphene/PDMS, respectively (Fig. 4a). It is important to note that graphene here acts as an electrode, cathode for Ni, and anode for MXene deposition. We first demonstrated the deposition of Ni from ammonium nickel (II) sulfate hexahydrate solution. Ni is an important electrode [39], catalyst [40], and EMI shielding metal [41]. Fig. 4b shows a uniform Ni film (the silver-white region) formed on the graphene surface. SEM images of the top (Fig. 4c) and cross-sectional views (Fig. 4d) show a densely packed Ni layer (~500 nm thick). We have also demonstrated the integration of MXene ($Ti_3C_2T_x$; T_x represents the surface terminations), a vital member of the 2D materials family with extremely high electrical conductivity and hydrophilic surface [42]. Because the MXene surface is negatively charged in the solution [43], graphene/PDMS is used as the anode. After the deposition of MXene, the substrate color changed to light purple, as shown in Fig. 4e. Similar to graphene assembly, most MXene flakes are parallel to the PDMS substrate, as shown in Figs. 4f and 4g. To validate the potential applications of these hierarchical devices, we have demonstrated two functions. Depositing Ni and MXene can significantly increase the conductivity of the assembled layer leading to ultrathin flexible EMI shielding materials. As

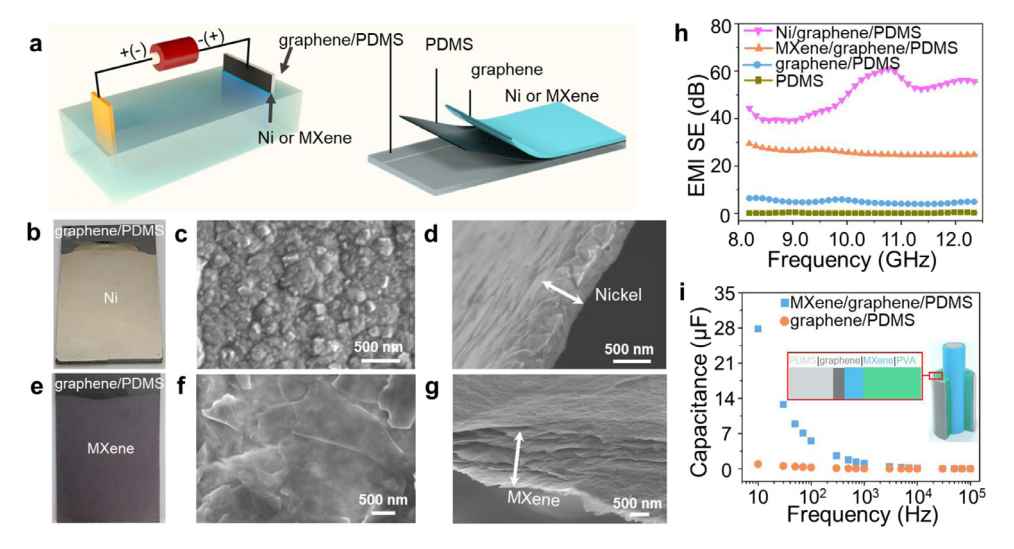


Fig. 4. Integrated hierarchical devices. (a) Schematic of the electroplating process for Ni and MXene coating (left) and the multilayer structure (right). (b) Digital image of Ni/graphene/PDMS. (c,d) Surface and cross-sectional morphologies of deposited Ni film. (e) Digital representation of MXene/graphene/PDMS. (f,g) Surface and cross-sectional morphologies of deposited MXene film. (h) EMI shielding performance for the integrated hierarchical structures in the X-band (8.2-12.4 GHz). (i) Dependency of capacitance on frequency for two different flexible solid-state electrochemical capacitors using graphene/PDMS and MXene/Gr/PDMS as the electrodes, respectively.

shown in Fig. 4h, in comparison with average EMI shielding effectiveness (SE) (see Supplementary Information) of 0.4 dB for PDMS sheet (1 mm thick) and 4.9 dB for graphene (~ 100 nm for each graphene layer)/PDMS 20-layer sheet in the X-band (8.2-12.4 GHz), 1 µm thick MXene on graphene/PDMS increased the average EMI SE to 25.7 dB, and 500 nm thick Ni on graphene/PDMS shows average EMI SE of 49.8 dB. Both of them meet the commercial standard for EMI shielding (EMI SE > 20 dB). Although this value of MXene film is relatively lower than the samples prepared by some well-optimized coating techniques [28] (e.g. ~40 dB for 1 µm thick filtered film), we believe the performance can be further improved by optimizing the SDC process and electroplating parameters. More importantly, our process provides a new route making functional multilayer coatings. Another example is a solid-state flexible electrochemical capacitor utilizing the excellent conductivity and large surface area of MXene and graphene. Two electrodes, MXene/graphene/PDMS and graphene/PDMS, were compared using PVA/KOH gel as the electrolyte. The dependency of the capacitance on frequency under the bias of 1 V is shown in Fig. 4i. The specific gravimetric capacitance of the MXene/graphene/PDMS device is calculated as 75.4 mF/g, which is around 10 times the value for graphene/PDMS devices (7.5 mF/g) at the frequency of 10 Hz.

4. Conclusions

We have demonstrated a new affordable and eco-friendly manufacturing concept that encompasses the lifecycle of nanomaterials-based flexible electronics from high-throughput device fabrication to device repair and regeneration. The developed method enables the interfacial energy driven assembly of hydrophobic particles on a hydrophobic substrate from aqueous dispersions in water, assisted by the kinetic energy of sonomatter interaction. This unique strategy transforms the dip-coating technology into a fast, high-throughput and eco-friendly SDC manufacturing process with a low energy consumption. The sono-healing method can be used to repair damaged films and nano-devices. This work not only establishes a novel strategy for assembly and repair of nanomaterial films, but also opens a new field of research. The SDC process can be integrated with other deposition technologies. As a proof of concept, we showed the integration of SDC with electroplating and deposited nickel and Ti₃C₂T_x MXene films onto graphene. Those hybrids showed excellent electromagnetic interference shielding ability and very good electrochemical performance. We believe this manufacturing concept will inspire further technology innovation in the advanced manufacturing of nanomaterial-based devices.

Declaration of Competing Interest

U.S. Provisional Patent. Appl. No.: 63/135,872.

Data availability

The data that support the findings of this study are available from the corresponding authors on request.

Credit authorship contribution statement

Dong Zhou: Conceptualization, Data curation, Formal analysis, Investigation, Methodology, Resources, Validation, Visualization, Writing-Original Draft. Meikang Han: Formal analysis, Investigation, Resources, Writing-review & editing. Bchara Sidnawi: Methodology, Formal analysis, Writing-review & editing. Qianhong Wu: Methodology, Formal analysis, Funding acquisition, Writing-review & editing. Yury Gogotsi: Formal analysis, Investigation, Resources, Funding acquisition, Writing-review & editing. Bo Li: Conceptualization, Data curation, Funding acquisition, Methodology, Resources, Supervision, Project administration, Writing-review & editing.

Acknowledgments

D.Z, and B.L. were partially supported by the National Science Foundation CMMI Advanced Manufacturing Program under Award # 2003077 and the startup fund of Villanova University. Q.W. and B.S. were partially supported by the National Science Foundation CBET Fluid Dynamics Program under Award #1511096. M.H. and Y.G. were supported by Murata, Japan. Acknowledgments go to Dr. Jie He at the University of Connecticut for the kind donation of the PMMA nanoparticles, Mr. Liang Zhao at Villanova University for some sample preparation, Dr. Calvin Li at Villanova University for the help in contact angle measurement, Dr. Xuemei Cheng at Bryn Mawr College for the help in photolithography and Dr. Emily Carson at Villanova University for language support.

Supplementary materials

Supplementary material associated with this article can be found, in the online version, at doi:10.1016/j.apmt.2021.100956.

References

- [1] D.-Y. Khang, J. Xiao, C. Kocabas, S. MacLaren, T. Banks, H. Jiang, Y.Y. Huang, J.A. Rogers, Molecular scale buckling mechanics in individual aligned single-wall carbon nanotubes on elastomeric substrates, Nano. Lett 8 (2008) 124-130.
- [2] G. Eda, M. Chhowalla, Graphene-based composite thin films for electronics, Nano Lett. 9 (2009) 814–818.
- [3] S. Bae, H. Kim, Y. Lee, X. Xu, J.-S. Park, Y. Zheng, J. Balakrishnan, T. Lei, H.R. Kim, Y.I. Song, Roll-to-roll production of 30-inch graphene films for transparent electrodes, Nat. Nanotechnol. 5 (2010) 574.
- [4] K. Dong, X. Peng, Z.L. Wang, Fiber/fabric-based piezoelectric and triboelectric nanogenerators for flexible/stretchable and wearable electronics and artificial intelligence, Adv. Mater. 32 (2020) 1902549.
- [5] Z. Ling, C.E. Ren, M.-Q. Zhao, J. Yang, J.M. Giammarco, J. Qiu, M.W. Barsoum, Y. Gogotsi, Flexible and conductive MXene films and nanocomposites with high capacitance, Proc. Natl. Acad. Sci. U.S.A. 111 (2014) 16676–16681.
- [6] H.E. Lee, D. Lee, T.-I. Lee, J.H. Shin, G.-M. Choi, C. Kim, S.H. Lee, J.H. Lee, Y.H. Kim, S.-M. Kang, Wireless powered wearable micro light-emitting diodes, Nano Energy 55 (2019) 454–462.
- [7] G.-H. Lee, H. Moon, H. Kim, G.H. Lee, W. Kwon, S. Yoo, D. Myung, S.H. Yun, Z. Bao, S.K. Hahn, Multifunctional materials for implantable and wearable photonic healthcare devices, Nat. Rev. Mater. 5 (2020) 149–165.
- [8] C.S. Haines, M.D. Lima, N. Li, G.M. Spinks, J. Foroughi, J.D. Madden, S.H. Kim, S. Fang, M.J. De Andrade, F. Göktepe, Artificial muscles from fishing line and sewing thread, Science 343 (2014) 868–872.
- [9] M.A. Ng, L.T. Hartadi, H. Tan, C.P. Poa, Efficient coating of transparent and conductive carbon nanotube thin films on plastic substrates, Nanotechnology 19 (2008) 205703.
- [10] C.-P. Lee, K.-Y. Lai, C.-A. Lin, C.-T. Li, K.-C. Ho, C.-I. Wu, S.-P. Lau, J.-H. He, A paper-based electrode using a graphene dot/PEDOT: PSS composite for flexible solar cells, Nano Energy 36 (2017) 260–267.
- [11] W. Hong, Y. Xu, G. Lu, C. Li, G. Shi, Transparent graphene/PEDOT-PSS composite films as counter electrodes of dye-sensitized solar cells, Electrochem. Commun. 10 (2008) 1555–1558.
- [12] B. Li, C. Zhang, B. Jiang, W. Han, Z. Lin, Flow-enabled self-assembly of large-scale aligned nanowires, Angew. Chem. Int. Ed. 54 (2015) 4250–4254.
- [13] S. Bauer, Flexible electronics: sophisticated skin, Nat. Mater. 12 (2013) 871–872.
- [14] S. Wu, J. Li, G. Zhang, Y. Yao, G. Li, R. Sun, C. Wong, Ultrafast self-healing nanocomposites via infrared laser and their application in flexible electronics, ACS Appl. Mater. Interfaces 9 (2017) 3040–3049.
- [15] N. Wu, Y.R. Shi, S.Y. Lang, J.M. Zhou, J.Y. Liang, W. Wang, S.J. Tan, Y.X. Yin, R. Wen, Y.G. Guo, Self-healable solid polymeric electrolytes for stable and flexible lithium metal batteries, Angew. Chem. Int. Ed. 58 (2019) 18146–18149.
- [16] T.P. Huynh, H. Haick, Self-healing, fully functional, and multiparametric flexible sensing platform, Adv. Mater. 28 (2016) 138–143.
- [17] S.J. Benight, C. Wang, J.B. Tok, Z. Bao, Stretchable and self-healing polymers and devices for electronic skin, Prog. Polym. Sci. 38 (2013) 1961–1977.
- [18] J. Tan, L. Looney, M. Hashmi, Component repair using HVOF thermal spraying, I. Mater. Process. Technol. 92 (1999) 203–208.
- [19] T. Gong, X. Zhang, Y. Fu, G. Zhou, H. Chi, T. Li, A facile fabrication of colorimetric graphene oxide reflecting films for ultrasensitive optical gas sensing, Sensor Actuat. B-Chem. 261 (2018) 83–90.
- [20] N.-K. Chang, C.-C. Su, S.-H. Chang, Fabrication of single-walled carbon nanotube flexible strain sensors with high sensitivity, Appl. Phys. Lett. 92 (2008) 063501.

- [21] E.Y. Jang, T.J. Kang, H.W. Im, D.W. Kim, Y.H. Kim, Single-walled carbon-nanotube networks on large-area glass substrate by the dip-coating method, Small 4 (2008) 2255–2261.
- [22] B. Li, H.Y. Jung, H. Wang, Y.L. Kim, T. Kim, M.G. Hahm, A. Busnaina, M. Upmanyu, Y.J. Jung, Ultrathin SWNT films with tunable, anisotropic transport properties, Adv. Funct. Mater. 21 (2011) 1810–1815.
- [23] F. Mirri, A.W. Ma, T.T. Hsu, N. Behabtu, S.L. Eichmann, C.C. Young, D.E. Tsentalovich, M. Pasquali, High-performance carbon nanotube transparent conductive films by scalable dip coating, ACS Nano 6 (2012) 9737–9744.
- [24] R. Ashiri, A. Nemati, M.S. Ghamsari, Crack-free nanostructured BaTiO₃ thin films prepared by sol–gel dip-coating technique, Ceram. Int. 40 (2014) 8613–8619.
- [25] P. Salles, D. Pinto, K. Hantanasirisakul, K. Maleski, C.E. Shuck, Y. Gogotsi, Electrochromic effect in titanium carbide MXene thin films produced by dip-coating, Adv. Funct. Mater. 29 (2019) 1809223.
- [26] R. Dabirian, V.H. Guerrero, D.C.L. Matovelle, L.J. Segura, Mechanical and electronic systems of an open source based spin and dip coater, Rev. Politécnica 37 (2016) 53 -53.
- [27] D.C. Marcano, D.V. Kosynkin, J.M. Berlin, A. Sinitskii, Z. Sun, A. Slesarev, L.B. Alemany, W. Lu, J.M. Tour, Improved synthesis of graphene oxide, ACS Nano 4 (2010) 4806–4814.
- [28] M. Han, C.E. Shuck, R. Rakhmanov, D. Parchment, B. Anasori, C.M. Koo, G. Friedman, Y. Gogotsi, Beyond Ti₃C₂Tx: MXenes for electromagnetic interference shielding, ACS Nano 14 (2020) 5008–5016.
- [29] J. Kim, S. Kwon, D.-H. Cho, B. Kang, H. Kwon, Y. Kim, S.O. Park, G.Y. Jung, E. Shin, W.-G. Kim, Direct exfoliation and dispersion of two-dimensional materials in pure water via temperature control, Nat. Commun. 6 (2015) 8294.
- [30] F. Petersson, A. Nilsson, H. Jönsson, T. Laurell, Carrier medium exchange through ultrasonic particle switching in microfluidic channels, Anal. Chem. 77 (2005) 1216–1221.
- [31] N. Nama, R. Barnkob, Z. Mao, C.J. Kähler, F. Costanzo, T.J. Huang, Numerical study of acoustophoretic motion of particles in a PDMS microchannel driven by surface acoustic waves, Lab. Chip 15 (2015) 2700–2709.
- [32] P.B. Muller, R. Barnkob, M.J.H. Jensen, H Bruus, A numerical study of microparticle acoustophoresis driven by acoustic radiation forces and streaming-induced drag forces, Lab. Chip 12 (2012) 4617–4627.
- [33] D.G. Shchukin, E. Skorb, V. Belova, H. Moehwald, Ultrasonic cavitation at solid surfaces, Adv. Mater. 23 (2011) 1922–1934.
- [34] D. Zhou, J. Hao, A. Clark, K. Kim, L. Zhu, J. Liu, X. Cheng, B. Li, Sono-assisted surface energy driven assembly of 2D materials on flexible polymer substrates: a green assembly method using water, ACS Appl. Mater. Interfaces 11 (2019) 33458–33464.
- [35] M. Mastrangeli, W. Ruythooren, C. Van Hoof, J.-P. Celis, Conformal dip-coating of patterned surfaces for capillary die-to-substrate self-assembly, J. Micromech. Microeng. 19 (2009) 045015.
- [36] A.A. Darhuber, S.M. Troian, J.M. Davis, S.M. Miller, S. Wagner, Selective dip-coating of chemically micropatterned surfaces, J. Appl. Phys. 88 (2000) 5119–5126.
- [37] Y. Wang, T.J. McCarthy, Dip-coating deposition on chemically patterned surfaces: a mechanistic analysis and comparison with topographically patterned surfaces, Langmuir 30 (2014) 2419–2428.
- [38] B. Sidnawi, D. Zhou, B. Li, Q. Wu, A physics-based statistical model for nanoparticle deposition, J. Appl. Phys, 2021 In press.
- [39] A. Lasia, A. Rami, Kinetics of hydrogen evolution on nickel electrodes, J. Electroanal. Chem. Interf. Electrochem. 294 (1990) 123–141.
- [40] J. Guo, H. Lou, H. Zhao, D. Chai, X. Zheng, Dry reforming of methane over nickel catalysts supported on magnesium aluminate spinels, Appl. Catal., A-Gen 273 (2004) 75–82.
- [41] S.-S. Tzeng, F.-Y. Chang, EMI shielding effectiveness of metal-coated carbon fiber-reinforced ABS composites, Mater. Sci. Eng., A 302 (2001) 258–267.
- [42] B. Anasori, Y. Gogotsi, 2D Metal Carbides and Nitrides (MXenes), Springer, 2019.
- [43] K. Maleski, V.N. Mochalin, Y. Gogotsi, Dispersions of two-dimensional titanium carbide MXene in organic solvents, Chem. Mater. 29 (2017) 1632–1640.